Macromolecules
COMMUNICATION TO THE EDITOR

DOI: 10.1021/ma902357s

Hierarchically Ordered Montmorillonite Block Copolymer Brushes

Ross E. Behling, Lynn M. Wolf, and Eric W. Cochran*

Department of Chemical and Biological Engineering, Iowa State University, Ames, Iowa 50011-2230

Received October 22, 2009
Revised Manuscript Received January 13, 2010

Block copolymers (BCPs) have been known for decades to offer an easily tunable method for producing self-assembled structures with length scales on the order of nanometers to tens of nanometers. More recently, the community has shown significant interest in exploiting the properties of BCP self-assembly to tailor the spatial and orientational distribution of nanoscale filler materials,[1] with targeted applications ranging from high-density storage devices,[2,3] to organic electronics,[4−6] to optical devices,[7,8] and to separation devices/catalytic membranes.[9−11]

From a commercial perspective, currently the most important class of polymer nanocomposites features layered silicates—typically montmorillonite (MMT)—suspended in a matrix of homopolymer. This combination of materials yields dramatically enhanced mechanical, barrier, and thermal properties compared to the neat homopolymer.[12] The degree to which these enhancements may be realized depends strongly on the morphology of clay inclusions and the clay−polymer interactions at the interphase.[13−15] Many studies have treated the problem of optimizing the dispersion of the clays within the polymer matrix.[16−19] The degree of dispersion and the spatial/orientational distribution of the particles in these systems are largely governed by the strong shear fields imposed on the system during processing. Typically this yields a distribution of particle aggregates and exfoliated particles, isotropically distributed throughout the system. The most successful examples to date of nanoparticle inclusion have nanoparticles functionalized with homopolymer and then dispersed in a BCP host matrix. Bockstaller et al. reviewed the successful inclusion of gold, silica, and montmorillonite (MMT) particles using this technique, providing an excellent overview of how BCPs can be employed to control nanoparticle dispersion and orientation.[1,20] Significantly, physical blending with nanoclays has not yet yielded any greater degree of control of the particle distribution than traditional homopolymer nanocomposites (NCPs).[21] This is evidently due to the difficulty of overcoming the strong particle−particle interactions and the disparity between the particle size, ≈100−300 × 1 nm, and typical BCP domain sizes, ≈10−50 nm.

A relatively unexplored alternative approach to nanocomposite formulation is to dispense with the matrix altogether by integrating it directly with the filler particle. For example, Gianellis and others have used this idea leading to the discovery of nanoparticle fluids by the attachment of oligomers to colloidal particles.[22] We have discovered that aggregation and particle distribution limitations can be circumvented by directly grafting BCPs to the silicate surface, effectively encapsulating the filler particle in a dense brush layer. Krishnamoorti and Vaia have speculated that "...block copolymers and other structured polymers onto the surfaces of nanoparticles can alter significantly the natural topologies adopted by those materials and therefore lead to interesting characteristics".[23] We find that this is indeed the case, with new emergent physics from the synergism generated by the combination of polymer brushes, nanoparticles, and block copolymer self-assembly. In this system the relationship between matrix and filler is uniquely dictated by molecular design, and the resultant system represents a distinct class of self-organizing materials. The thermodynamics of these MMT block copolymer brush (MBB) systems reflect the consequences of microphase separation constrained by the brush extension and the connectivity of the chain ends to the semiflexible MMT substrate. The morphology of these materials is intrinsically hierarchical, with characteristic length scales prescribed by the supporting MMT particle (Figure 1a), the polymer chain dimensions (Figure 1b), and the chain stretching/interfacial curvature imposed by microphase separation (Figure 1c). In this Communication we present and interpret examples of the hierarchically ordered structures that form as a consequence of these multiple length scales.

Montmorillonite clay was generously supplied by Southern Clay Products Inc. Based on the ion exchange capacity, 92 mequiv/100 g, and measurements of the specific surface area,[24] MMT contains ≈1 site/nm^2. MMT was functionalized with a bromine-terminated alkylammonium surfactant (Figure 1a) and was subsequently polymerized via surface-initiated ATRP (SI-ATRP) to yield polystyrene (Figure 1b) and poly(styrene-*block*-*tert*-butyl acrylate) brushes (Figure 1c) as described in detail elsewhere.[25] We refer to MMT-*graft*-poly(styrene) homopolymer brushes as MMT-X and MMT-*graft*-poly(styrene-*block*-*tert*-butyl acrylate) block copolymer brushes as MBB-X-Y; X refers to polystyrene (PS) and Y to poly(*tert*-butyl acrylate) (PtBA) number-average molecular weight (M_n) in kDa. MBBs were annealed at 150 °C *in vacuo* for over 96 h prior to being steady shear processed at 1^{-1} and 160−200 °C for 25 min on a TA Instruments ARES-LS1 strain-controlled rheometer in the parallel plate geometry under N_2. Ultrathin (≈100 nm) sections were obtained at −100 °C using a Leica Ultramicrotome Ultracut 125UCT with a Leica EM FCS cryo-stage. RuO_4-stained sections were examined on a Tecnai G^2 F20 scanning/transmission electron microscope at a high tension voltage of 200 kV. Length scale information was extracted from TEM images by a combination of line measurements taken using the Gatan DigitalMicrograph software and analysis of the azimuthal average of the discrete Fourier transform (DFT).

Part I of Figure 2 shows a series of TEM micrographs of ascending corona block length and fixed core block length, where the PtBA block was stained to enhance contrast. Figure 2a demonstrates partial phase separation as evidenced by 25−100 nm ellipsoidal "pockets" locally enriched in PS, distributed in a homogeneous PS/PtBA background. The mean distance between "pockets", as determined by DFT analysis, is 31 nm. MBB-44-64 (Figure 2b) features a corona block nearly twice the size of MBB-44-36 (Figure 2a) and exhibits a fully ordered morphology. Here the PS domains form an interpenetrating network characterized by domains ≈28 nm in diameter, separated on average by 51 nm with irregular connectivity. Further increasing the corona block size to nearly triple that of MBB-44-36, MBB-44-90 (Figure 2c) displays modulated cylindrical domains, 90 nm in diameter, of PS and PtBA interpenetrating in a manner reminiscent of wormlike micelles that are observed in dilute solutions of amphiphilic BCPs.[26] Part II of Figure 2 depicts structures nearly twice as large as those seen in part I of Figure 2. The composition of MBB-70-30 is roughly that of MBB-44-90 with reverse majority and minority components and comparable overall molecular

*Corresponding author. E-mail: ecochran@iastate.edu.

Published on Web 02/04/2010

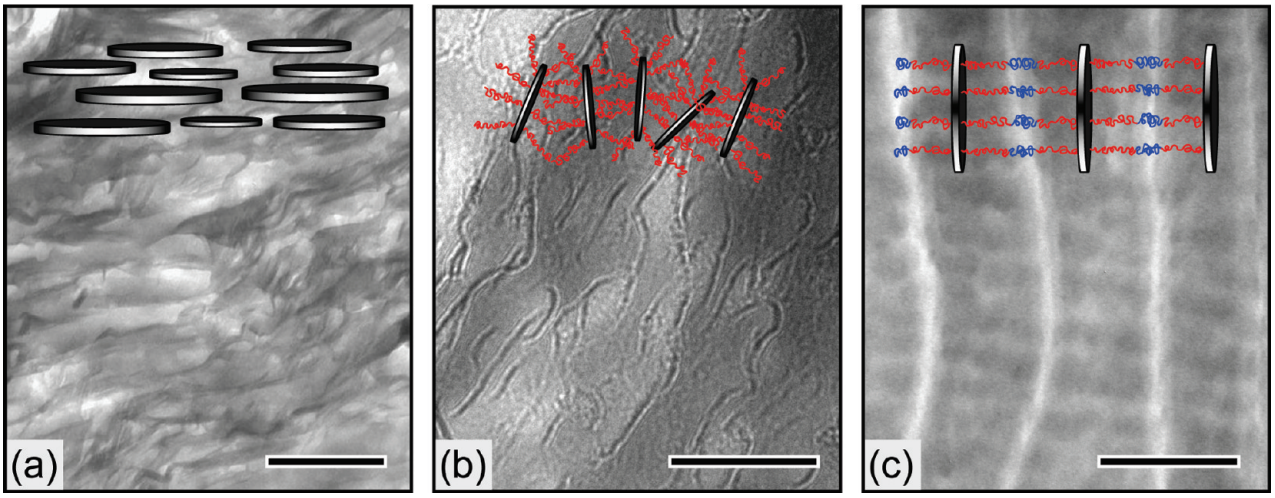

Figure 1. Representative TEM micrographs of (a) montmorillonite clay, (b) MMT-50, and (c) MBB-70-30 (processed with high-amplitude reciprocating shear), with the associated schematics of the unit structures. Red chains depict PS blocks, blue chains PtBA blocks, and gray MMT disks. Scale bar is 250 nm.

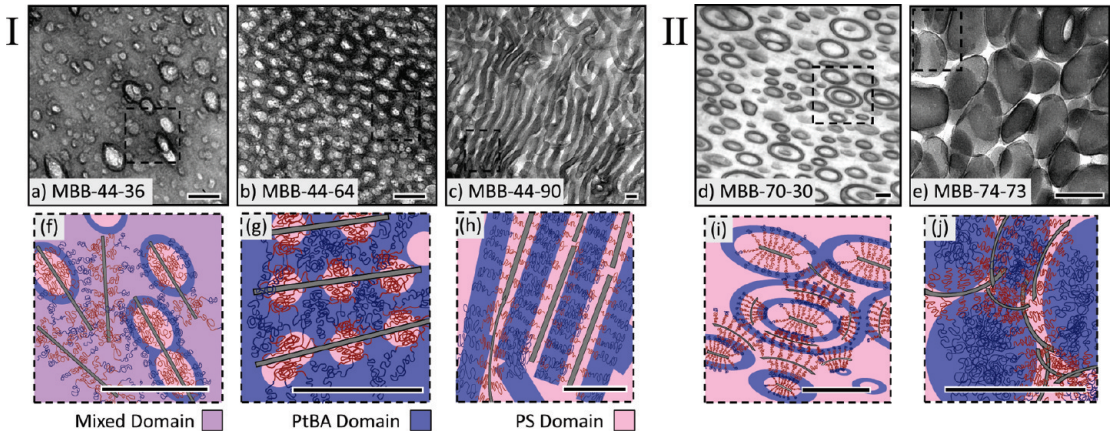

Figure 2. (a−e) Representative TEM micrographs of multiple NCP morphologies (a) MBB- 44-36, (b) MBB-44-64, (c) MBB-44-90, (d) MBB-70-30, and (e) MBB-74-73 with the associated schematics of the unit structures. Scale bars for micrographs and schematics are respectively identical; tBA domain stained with RuO_4 for contrast. (f−j) Schematic illustrations of the polymer/clay configuration suggested by the micrographs in the top row. (Part I) Scale bar is 100 nm. (Part II) Scale bar is 200 nm.

weights; however, the morphology of MBB-70-30 bears no resemblance to that of MBB-44-90. MBB-70-30 exhibits single and concentric tori of PtBA 25−35 nm thick that average 200 nm (450 nm) in the axial direction and 100 nm (200 nm) in the cross-axial direction. The nearly symmetric composition of MBB-74-73 is comprised of oblate PtBA ellipsoids averaging 250 nm in the major axis and 150 nm in the minor axis with ≈20% deviation in both axes.

To facilitate our interpretation of the unique progression of the morphology in these specimens, we first make a number of observations. One, the segregation strength χN, where χ is the Flory interaction parameter and N is the polymerization index, required to induce complete microphase separation in MBBs is significantly larger than that in analogous untethered AB diblocks. Two, the characteristic domain sizes in the structures spans an incredibly wide range—from 15 to 500 nm—whereas the brush M_n varies over a much smaller range, 80−150 kDa. This is in stark contrast to AB diblocks of comparable molar mass, where the feature sizes would be <50 nm. Three, the morphology is strongly dependent on the absolute brush polymerization index N, again in contrast to AB diblocks where the entire phase space is mapped by the chain composition f and χN. Four, the block sequence plays a key role in the evolution of the morphology.

Self-assembly in MBBs is intrinsically hierarchical due to the mixture of length scales fundamentally present in the system: the supporting MMT particle is discoidal with diameter on the order of 10^2 nm; polymers grafted to the MMT surface are constrained to have an interchain spacing on the order of 10^0 nm at the graft site, and the length scale of polymer microphase separation is dictated by the RMS end-to-end distance h. h is bounded by the contour length, on the order of 10^2 nm for the polymers considered here. The degree of chain stretching in these materials is significant and can be estimated through a qualitative calculation as depicted in Figure 3a: Consider an ideal MMT particle to be a disk with radius $R = 100$ nm, grafted with 50 kDa PS chains at a graft density $\rho_g = 1$ chains/nm^2. The volume of PS attached to this particle is then $V_{PS} = \pi R^2 \rho_g \bar{V}_{PS}$, where $\bar{V}_{PS} \approx 90$ nm^3/chain is the volume of a 50 kDa PS chain. Now suppose that r represents the maximum distance of PS from the MMT particle. Equating V_{PS} to the volume defined by the encapsulated particle depicted in Figure 3a yields $\rho_g \bar{V}_{PS} = \pi r^2/R + 2r$ with $r =$ 30.4 nm, ≈ 25% of the contour length. This implies an interparticle separation of ≈60 nm in strong qualitative agreement with the mean interparticle spacing of ≈50nm in MMT-50 (Figure 1b). Thus, for microphase separation to occur in MBBs, the system must accommodate additional chain stretching to form

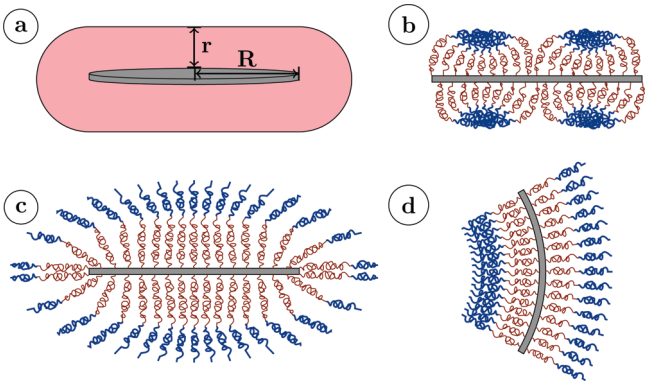

Figure 3. Schematic illustrations that describe the physics of MBB self-assembly. (a) Chains are strongly stretched since they are constrained to reside within the shaded volume, a distance r from the supporting MMT particle. At sufficient segregation strength this leads to either (b) intraparticle self-assembly or (c) interparticle self-assembly. This mode of phase separation is characterized by large domain spacing. (d) Interfacial curvature for interparticle self-assembly must be accompanied by bending of the supporting particle, requiring the symmetry of the mirror plane to be broken.

discrete domains. Consequently, MBB materials should require a significantly higher degree of segregation strength than the analogous untethered BCPs. MBB-44-36 (Figure 2a) is only partially ordered in spite of the 80 kDa size of the polymer brush and is consistent with this idea. Clearly, the weak ordering exhibited by MBB-44-36 demonstrates that this material is only weakly segregated even though $\chi N \gg 10.5$. As depicted schematically in Figure 2f, PS-rich domains are stable only near the PS−MMT interface; beyond this region, the additional entropic cost of phase separation is not sufficient to compensate for the enthalpic cost of remaining homogeneous. Consequently, the PS domain size in MBB-44-36 is thus governed by the MMT particle size whereas the interdomain spacing is dictated by the polymer molecular weight.

Complete phase separation begins to occur in MBB-44-64 where the PtBA block is sufficiently large to form distinct domains with diffuse PS/PtBA interfaces curved toward the minority PS regions as depicted in Figure 2g. This system evidently exhibits *intraparticle* phase separation, where the PS domains form within the plane defined by the MMT particle. Here phase separation is essentially constrained to occur within this plane, within a single MBB pseudoparticle; interactions with adjacent particles only occur to fill the overall void space. The domain spacing, 46 nm, is consistent with traditional diblock copolymers of comparable size.

In MBB-44-90 (Figure 2c), however, the larger PtBA block completely fills the space between opposing MBB surfaces, and we observe a fundamental difference in the way the system self-organizes. As a consequence of the formation of contiguous polymer microdomains, the supporting MMT particles are now also ordered, in contrast to MBB-44-64, and the dominant structural unit arises from *interparticle* assembly as illustrated in Figure 3c. In this system the characteristic length scale of MMT emerges directly in the microdomain structure as evidenced by the dramatic increase of the interdomain spacing of 46 nm in MBB-44-64 to 90 nm in MBB-44-90; that is, a 24% increase in the molecular weight induces a 96% increase in the domain spacing.

Similarly, increasing the size of the interior PS block also has a remarkable influence on the morphology. MBB-74-73 (Figure 2e) is similar in composition to MBB-44-36 and nearly double the molecular weight. The structure of MBB-74-73 again reflects interparticle self-assembly with an average domain size of 250 × 150 nm. Here intraparticle phase separation is not possible; the only mechanism by which the system can reduce unfavorable PS/PtBA interactions is through coherent ordering of the entire MBB particle, which is evidently responsible for the uncharacteristically large domain size. We observe the interparticle assembly mechanism in MBB-70-30 as well, where the corona PtBA block is the minority component. Here, an untethered diblock of identical composition would be expected to form PtBA cylinders, with the interfaces curved toward the minority phase. However, in MBB-70-30, the large core PS block is unable to provide this interfacial curvature locally. Rather, the concentrically arranged tori that appear in Figure 2d result from the long-range ordering of MBB particles and provide an alternative route to forming the interfacial curvature. The major axis diameter of these tori are as large as 500 nm, which is *larger* than that expressed by MBB-74-73 although the molecular weight is appreciably *smaller*. The tori thickness is ≈30 nm consistently throughout the specimen, expressing the length scale associated with the PtBA block size.

It is interesting to compare MBB-70-30 with MBB-44-90, which are nearly complementary in chemical composition and of similar molar mass, yet the differences in their morphology serves to illustrate the influence of the location of the minority block. In MBB-44-90 the minority block is the core, and its encapsulation with the majority corona block naturally promotes the formation of interfaces curved toward the PS domains and allows the formation of a nearly periodic structure. In contrast, there is no manner in which MBB-70-30 can tile space while forming interfaces curved toward the minority corona block.

The formation of curved interfaces through interparticle self-assembly requires the *bending* of the supporting MMT particles we depict schematically in Figure 3d, breaking the symmetry of the internal mirror plane defined by the MMT support. In neat BCPs, the interfacial curvature is the result of a precise balance between the enthalpic interactions, F^{int}, with the elastic energy contributed by chain stretching, F^{chain}. In MBBs, the introduction of the high-aspect ratio interface imposed by the clay particles should dampen the degree of curvature possible with the introduction of the clay bending energy F^{clay}. One may reasonably speculate, as in other quenched bilateral brush systems,[27] that this bending energy should dominate the system, and therefore, only lamellar configurations such as that appearing Figure 1c would be stable. MBB-44-90, MBB-70-30, and MBB-74-73 suggest otherwise by exhibiting interfaces with radii of curvature on the order of the estimated persistence length of MMT, ≈140 nm.[28] In homopolymer/MMT mixtures, Drummy et al. have observed clay platelets bent even more severely with the radius of curvature as small as 15 nm.[29] Clearly, while the bending stiffness of MMT is significant, ≈1.25 N m,[30] the energy increase with clay deformation is matched to that of the energy decrease to the relaxation of the polymer conformations accessible through bending. The precise mechanism for this spontaneous bending is thus likely a subtle consequence of a delicate energetic balance; we are currently developing a self-consistent field theoretic model of this system to quantitatively address this issue.

The interplay of F^{chain}, F^{int}, and F^{clay} lead to the rich polymer physics we observe in MBBs. MBBs represent a new class of materials capable of self-assembly into structures with length scales previously unaccessible to block copolymers of comparable molecular weights and unparalleled control of the spatial and orientational ordering of the filler particles. The physics of the MBB system are governed by the canonical parameters f and χN that pertain to AB diblocks; moreover, N and the block sequence play critical roles in the delicate balance of energies that lead to the mesophases we have observed. Important technological implications of these materials arise from two important features of MBBs: the length scales associated with ordered phases easily approach the microscopic range, and we expect

that the extremely strong degree of chain stretching may have a profound influence on physical properties.

These materials may lead to a new route to nonlinear optical materials owing to their ability to reach domain sizes on the order of visible light. For example, BCP domain spacings of 100−200 nm were previously only accessible by synthesizing lamellar diblocks (f = 0.50) of $M_{n,total}$ > 1000 kDa or using relatively smaller blocks of 200 kDa each and swelling the domains with homopolymer.[31] By comparison, MBBs can reach domain sizes as large as 150 nm at only 100 kDa. Finally, the high level of chain stretching in MBBs may offer a route to materials with elevated glass transition temperature or unprecedented degrees of crystallinity.

Acknowledgment. Acknowledgment for support of this research is made to the Donors of the American Chemical Society Petroleum Research Fund (PRF #48399-G7), the Camille and Henry Dreyfus New Faculty Award Program, and the National Science Foundation, DMR-0847515.

Supporting Information Available: Further experimental details and additional microscopy data. This material is available free of charge via the Internet at http://pubs.acs.org.

References and Notes

(1) Bockstaller, M. R.; Mickiewicz, R. A.; Thomas, E. L. *Adv. Mater.* **2005**, *17*, 1331.
(2) Arico, A. S.; Bruce, P.; Scrosati, B.; Tarascon, J.-M.; van Schalkwijk, W. *Nat. Mater.* **2005**, *4*, 366–377.
(3) Stoykovich, M. P.; Muller, M.; Kim, S. O.; Solak, H. H.; Edwards, E. W.; de Pablo, J. J.; Nealey, P. F. *Science* **2005**, *308*, 1442–1446.
(4) Jason, A. G.; Robert, E. C. *J. Appl. Polym. Sci.* **2004**, *91*, 3362–3368.
(5) Barber, J. R. P.; Gomez, R. D.; Herman, W. N.; Romero, D. B. *Org. Electron.* **2006**, *7*, 508–513.
(6) Balazs, A. C.; Emrick, T.; Russell, T. P. *Science* **2006**, *314*, 1107.
(7) Scott, B. J.; Wirnsberger, G.; Stucky, G. D. *Chem. Mater.* **2001**, *13*, 3140–3150.
(8) Yoon, J.; Lee, W.; L.Thomas, E. *MRS Bull.* **2005**, *30*, 721–726.
(9) Park, H. B.; Kim, J. K.; Nam, S. Y.; Lee, Y. M. *J. Membr. Sci.* **2003**, *220*, 59–73.
(10) Mauritz, K. A.; Mountz, D. A.; Reuschle, D. A.; Blackwell, R. I. *Electrochim. Acta* **2004**, *50*, 565–569.
(11) Cong, H.; Radosz, M.; Towler, B. F.; Shen, Y. *Sep. Purif. Technol.* **2007**, *55*, 281–291.
(12) Hussain, F.; Hojjati, M.; Okamoto, M.; Gorga, R. E. *J. Compos. Mater.* **2006**, *40*, 1511.
(13) Bartholmai, M.; Schartel, B. *Polym. Adv. Technol.* **2004**, *15*, 355.
(14) LeBaron, P. C.; Wang, Z.; Pinnavaia, T. J. *Appl. Clay Sci.* **1999**, *15*, 11.
(15) Fredrickson, G. H.; Bicerano, J. *J. Chem. Phys.* **1999**, *110*, 2181.
(16) Balazs, A. C.; Singh, C.; Zhulina, E.; Lyatskaya, Y. *Acc. Chem. Res.* **1999**, *32*, 651–657.
(17) Rong, W.; Feng, Q.; Hongdong, Z.; Yuliang, Y. *J. Chem. Phys.* **2003**, *118*, 9447–9456.
(18) Stretz, H. A.; Paul, D. R.; Li, R.; Keskkula, H.; Cassidy, P. E. *Polymer* **2005**, *46*, 2621–2637.
(19) Heinz, H.; Vaia, R. A.; Farmer, B. L. *J. Chem. Phys.* **2006**, *124*, 224713–9.
(20) Ha, Y.-H.; Kwon, Y.; Breiner, T.; Chan, E. P.; Tzianetopoulou, T.; Cohen, R. E.; Boyce, M. C.; Thomas, E. L. *Macromolecules* **2005**, *38*, 5170.
(21) Ren, J.; Silva, A. S.; Krishnamoorti, R. *Macromolecules* **2000**, *33*, 3739.
(22) Bourlinos, A.; Giannelis, E.; Zhang, Q.; Archer, L.; Floudas, G.; Fytas, G. *Eur. Phys. J. E* **2006**, *20*, 109–117.
(23) Krishnamoorti, R.; Richard, A. V. *J. Polym. Sci., Part B: Polym. Phys.* **2007**, *45*, 3252–3256.
(24) Shen, Y.-H. *Chemosphere* **2002**, *48*, 1075.
(25) Behling, R. E.; Williams, B. A.; Staade, B. L.; Wolf, L. M.; Cochran, E. W. *Macromolecules* **2009**, *42*, 1867.
(26) Won, Y. Y.; Paso, K.; Davis, H. T.; Bates, F. S. *J. Phys. Chem. B* **2001**, *105*, 8302.
(27) Birshtein, T. M.; Iakovlev, P. A.; Amoskov, V. M.; Leermakers, F. A. M.; Zhulina, E. B.; Borisov, O. V. *Macromolecules* **2007**, *41*, 478–488.
(28) Suter, J. L.; Coveney, P. V.; Greenwell, H. C.; Thyveetil, M.-A. *J. Phys. Chem. C* **2007**, *111*, 8248–8259.
(29) Drummy, L. F.; Koerner, H.; Farmer, K.; Tan, A.; Farmer, B. L.; Vaia, R. A. *J. Phys. Chem. B* **2005**, *109*, 17868–17878.
(30) Manevitch, O. L.; Rutledge, G. C. *J. Phys. Chem. B* **2004**, *108*, 1428–1435.
(31) Yoon, J.; Lee, W.; Thomas, E. L. *MRS Bull.* **2005**, *30*, 721.